Atmospheric Chemistry and Physics

Supporting Information for

Contributions of Lightning to Long-term Trends and Inter-annual Variability in Global Atmospheric Chemistry Constrained by Schumann Resonance Observations

Xiaobo Wang[1,2,3], Yuzhong Zhang[2,3], Tamás Bozóki[4,5], Ruosi Liang[1,2,3], Xinchun Xie[1,2,3], Shutao Zhao[1,2,3], Rui Wang[2,3], Yujia Zhao[1,2,3], and Shuai Sun[1,2,3]

[1]College of Environmental and Resource Sciences, Zhejiang University, Hangzhou, Zhejiang, China

[2]Key Laboratory of Coastal Environment and Resources of Zhejiang Province, School of Engineering, Westlake University, Hangzhou, China

[3]Institute of Advanced Technology, Westlake Institute for Advanced Study, Hangzhou, China

[4]HUN-REN Institute of Earth Physics and Space Science, Sopron, Hungary

[5]Department of Geophysics and Space Science, Institute of Geography and Earth Sciences, ELTE Eötvös Loránd University, Budapest, Hungary

Corresponding author: Yuzhong Zhang (zhangyuzhong@westlake.edu.cn)

This supplemental information contains 1 text section and 5 figures, totaling 8 pages including the cover page.

Text S1. Evaluation of the change of high-altitude NO_2 concentrations with TROPOMI observations by cloud-slicing technique

We evaluate the performance of SR observation method with the space-based tropospheric monitoring instrument (TROPOMI) NO_2 observations by cloud-slicing technique (Figures S3a-d and S4a-b). We find global lightning activity and LNO_x emissions based on SR observations have most anomaly (~10%) in 2020 relative to 2019, with the most significant decline in September-November (Figure S3a). So, we further analyze zonal sensitivity of lightning-driven anomalies of global NO_2 concentrations based on SR observations in September-November 2020 relative to 2019, and find that the NO_2 concentrations have significant anomalies in the Central Africa, the Northern South America, the Southeastern North America and the Islands of Indonesia (Figure S3b). We consider the following facts: (1) approximately half of global wildfire take place in the Central Africa (van der Werf et al., 2017); (2) the Southeastern North America region is significantly impacted by human activities (Teoh et al., 2024); and (3) the Islands of Indonesia region is also greatly affected by wildfire and anthropogenic emissions (Teoh et al., 2024; van der Werf et al., 2017). This implies that lightning based on SR observations is indeed not the primary contributor to NO_2 concentrations in these regions. We further find the lightning-driven NO_2 concentrations constrained by SR observations have most decline (-20.1±0.5 ppt) in the upper troposphere (300–100 hPa) of Northern South America in this time (Figure S3c), while the effects of wildfire emissions are smaller (4.5±0.1 ppt). Therefore, we choose the upper troposphere (300–100 hPa) of Northern South America region for subsequent evaluation with TROPOMI NO_2 observations by cloud-slicing technique.

TROPOMI NO_2 data are from the level-2 offline (OFFL) product (version 01-03-02) of the Sentinel-5P Pre-Operations Data Hub (S5P Data Hub, 2020). We retrieve upper troposphere (300–100 hPa) NO_2 mean concentrations at 2° × 2.5° in September-November 2019 and 2020 from TROPOMI using FRESCO-S cloud information by applying the cloud-slicing algorithm introduced by Marais et al. (2021) and corresponding Python code (https://zenodo.org/records/3979211; Accessed on 23 June

2024) released by Marais and Roberts (2020). Furthermore, we also made corresponding adjustments based on the improvements in the code afterwards (https://zenodo.org/records/4058442; Accessed on 23 June 2024): retaining retrieved NO_2 data greater than 200 ppt and outside the 10th-90th percentile range; changing "npnts < 100" to "npnts < 50".

The cloud-slicing TROPOMI NO_2 mean concentrations at 300–100 hPa in September-November 2019 and 2020 are shown in Figures S4a-b. We can find there are enough the amount of result retrieved to represent the NO_2 concentrations in the upper troposphere (300–100 hPa) of Northern South America. We further apply 1,000,000 Monte Carlo simulations to calculate the anomalies of NO_2 mean concentrations in this region from the base simulation with the OP method, the updated simulation with lightning based on SR observations and TROPOMI NO_2 observations by cloud-slicing technique (Figure 7a). We find the anomalies of NO_2 mean concentrations from the updated simulation match more well with TROPOMI NO_2 observations by cloud-slicing technique than the base simulation.

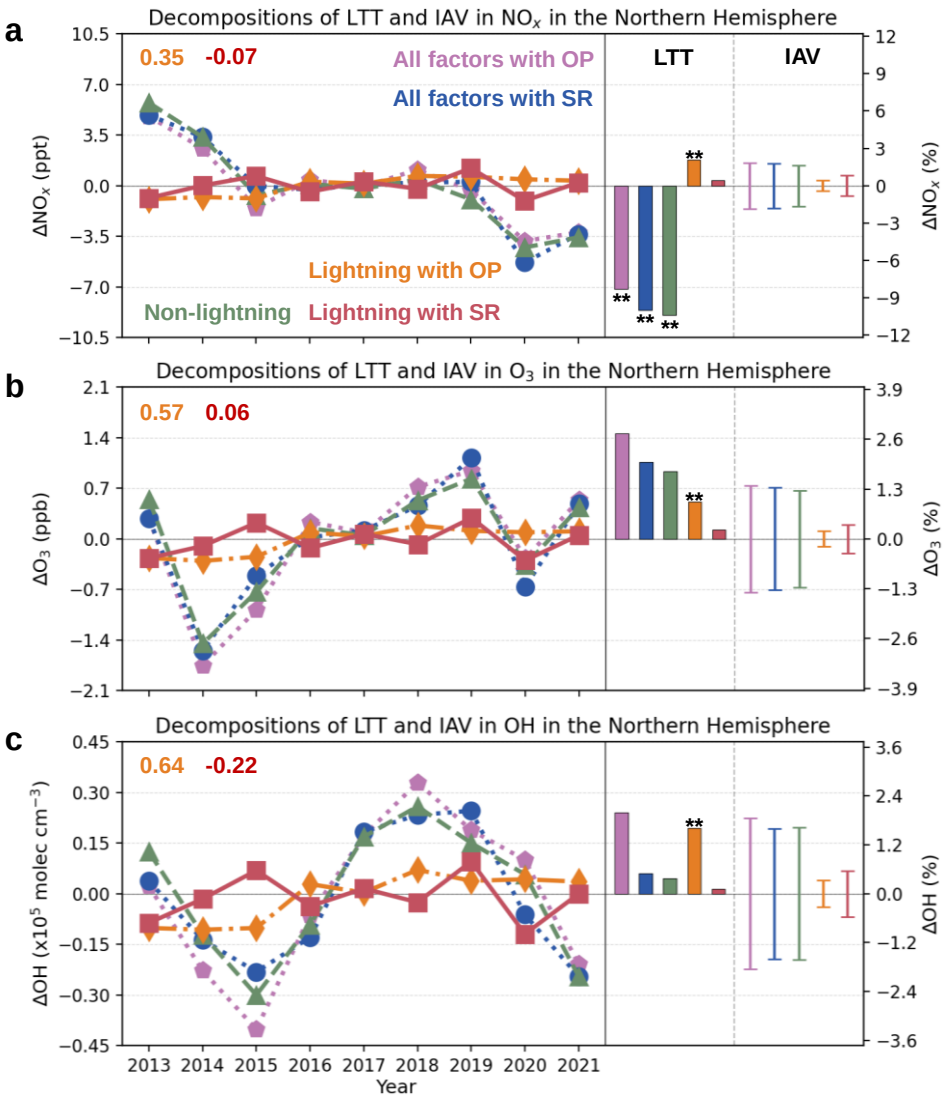

Figure S1. Anomalies, LTT and IAV of NO_x (a), O_3 (b) and OH (c) in the Northern Hemisphere, and their decompositions into lightning and non-lightning factors during 2013–2021. LTT values are reported in the unit of % dec^{-1}. ** denotes significant trends ($P < 0.05$) and * moderately significant trends ($0.05 \leq P < 0.1$). Correlation coefficients between the lightning (OP: orange; SR: red) and non-lightning contribution are denoted in the upper left of each panel. Shown in the upper left of each panel are correlation coefficients between the annual anomalies (with LTTs removed) of lightning (OP: orange; SR: red) and non-lightning contributions.

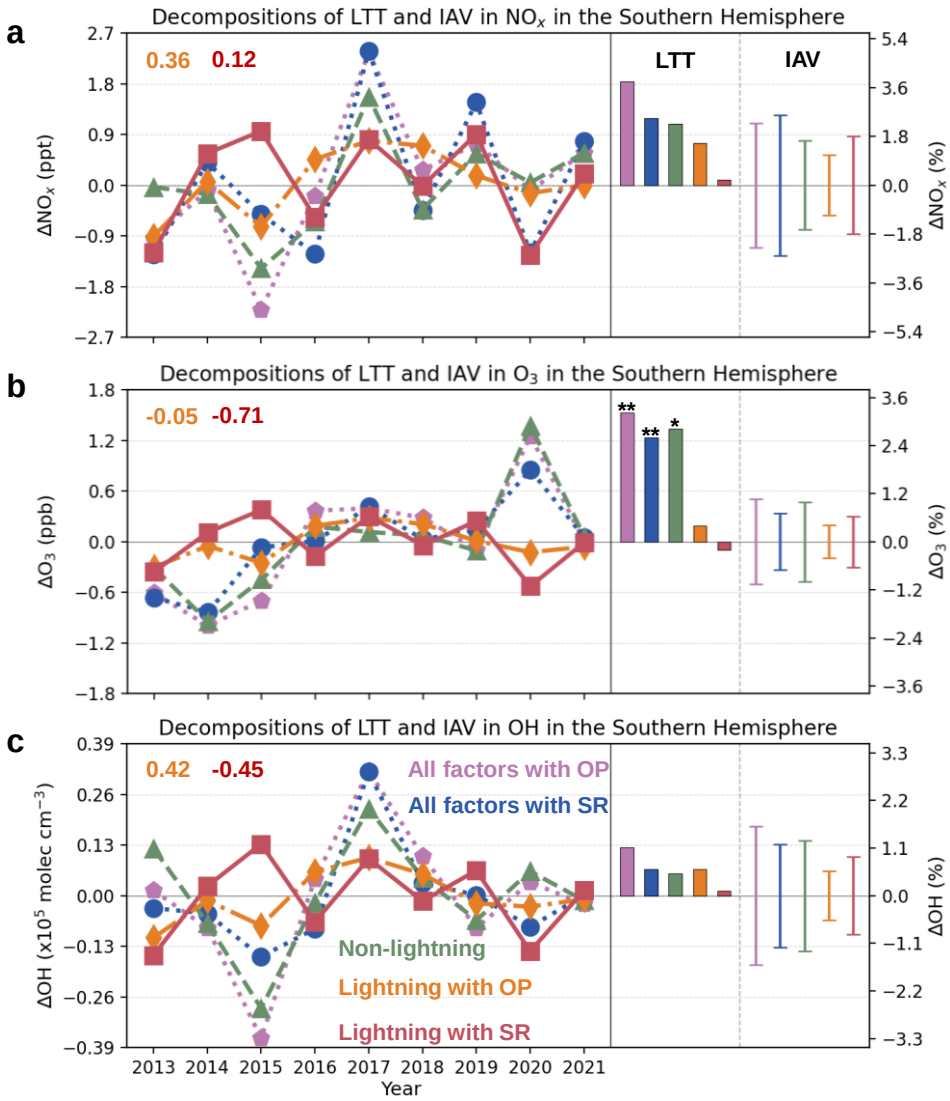

Figure S2. Anomalies, LTT and IAV of NO_x (a), O_3 (b) and OH (c) in the Southern Hemisphere, and their decompositions into lightning and non-lightning factors during 2013–2021. LTT values are reported in the unit of % dec^{-1}. ** denotes significant trends ($P < 0.05$) and * moderately significant trends ($0.05 \leq P < 0.1$). Correlation coefficients between the lightning (OP: orange; SR: red) and non-lightning contribution are denoted in the upper left of each panel. Shown in the upper left of each panel are correlation coefficients between the annual anomalies (with LTTs removed) of lightning (OP: orange; SR: red) and non-lightning contributions.

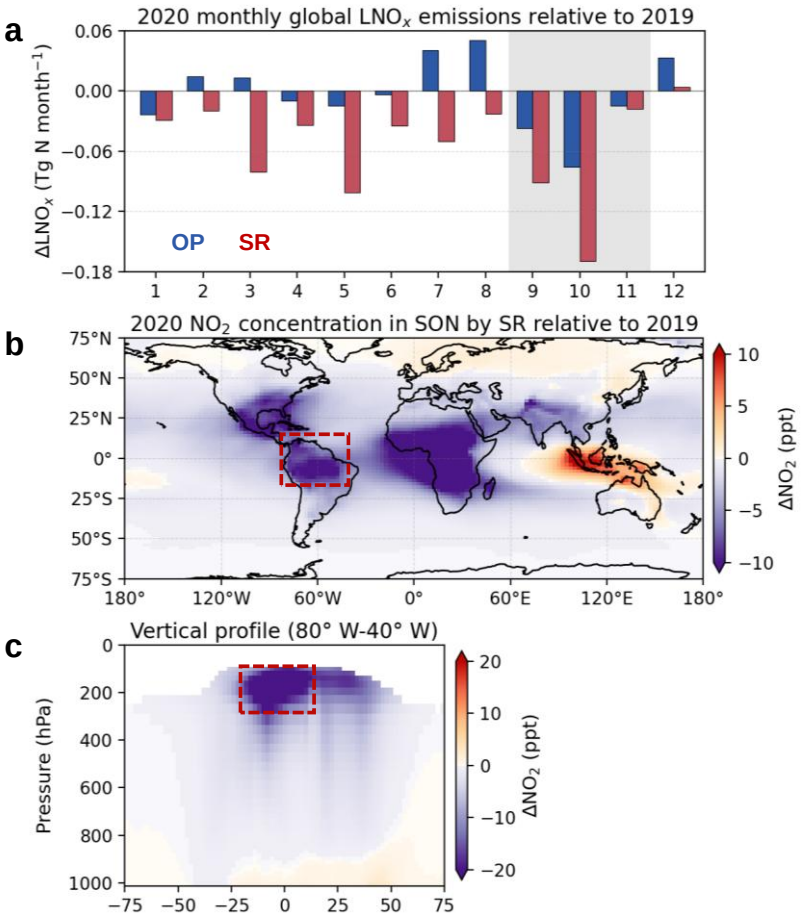

Figure S3. (a) Monthly changes in global LNO_x emissions based on the OP method and SR observations in 2020 relative to 2019. The plan (b) and section between 80° W and 40° W (c) of lightning-driven anomalies of NO_2 concentrations based on SR observations in September-November 2020 relative to 2019. The red boxes indicate the sensitive zone for subsequent evaluation.

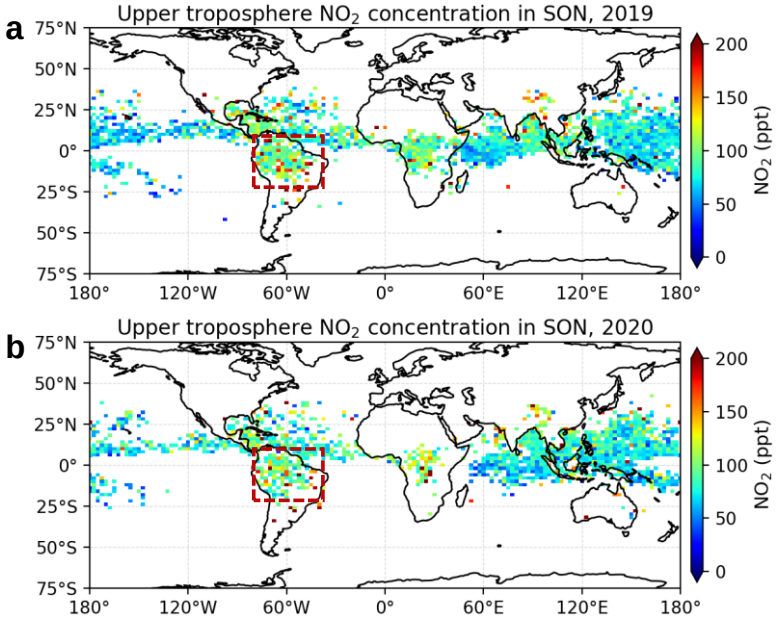

Figure S4. NO_2 mean concentrations in the upper troposphere (300–100 hPa) in September-November 2019 (a) and 2020 (b) from TROPOMI observations by the cloud-slicing technique. The red boxes indicate the sensitive zone for evaluation.

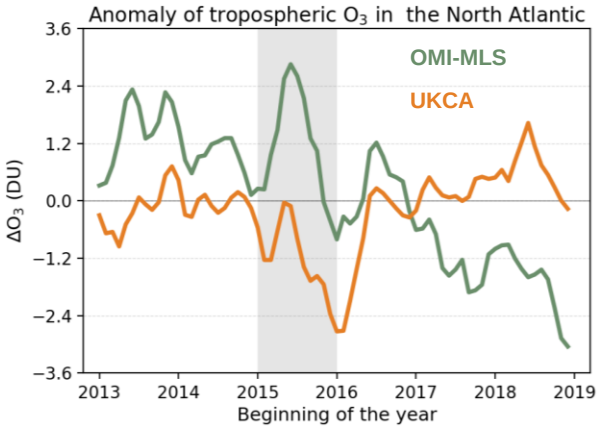

Figure S5. Time series anomalies of tropospheric O_3 observed by OMI-MLS and modelled by UKCA in the North Atlantic (0–60° N and 100° W–30° E) referenced from Figure 11a of Russo et al., (2023). The gray-shade background highlights the considerable discrepancy of changes in tropospheric O_3 in 2015 between observations and model evaluation.

References

Marais, E. A., et al. (2021). New observations of NO_2 in the upper troposphere from TROPOMI, *Atmospheric Measurement Techniques*, *14*(3), 2389-2408, doi:10.5194/amt-14-2389-2021.

Marais E. A., and J. F. Roberts (2020). eamarais/erc-uptrop: tropomi-ut-no2-1.1.0 (1.1.0). Zenodo. doi:10.5281/zenodo.4058442.

Russo, M. R., B. J. Kerridge, N. L. Abraham, J. Keeble, B. G. Latter, R. Siddans, J. Weber, P. T. Griffiths, J. A. Pyle, and A. T. Archibald (2023). Seasonal, interannual and decadal variability of tropospheric ozone in the North Atlantic: comparison of UM-UKCA and remote sensing observations for 2005-2018, *Atmospheric Chemistry and Physics*, *23*(11), 6169-6196, doi:10.5194/acp-23-6169-2023.

Teoh, R., Z. Engberg, M. Shapiro, L. Dray, and M. E. J. Stettler (2024). The high-resolution Global Aviation emissions Inventory based on ADS-B (GAIA) for 2019-2021, *Atmospheric Chemistry and Physics*, *24*(1), 725-744, doi:10.5194/acp-24-725-2024.

van der Werf, G. R., et al. (2017). Global fire emissions estimates during 1997-2016, *Earth System Science Data*, *9*(2), 697-720, doi:10.5194/essd-9-697-2017.